

## Influence of CaCO<sub>3</sub> micro- and nano-particles on the structure and properties of Nylon-66

Aboutaleb Ghadami, Jadval Ghadam

Faculty of Engineering, Departments of Chemical & Petroleum Engineering, Yasouj Branch, Islamic Azad University, Yasouj, I.R. IRAN

Received June 26, 2015; Revised September 10, 2015

Polyamide-66 (PA66)/CaCO<sub>3</sub> micro- and nano-composites were successfully prepared by polymer solution method. The material was characterized by XRD, SEM, FTIR, UV-VIS, DSC, Viscometry technique and UTM. The XRD results of composites have suggested that the  $\alpha$ -crystalline form is thermodynamically more stable and has a higher modulus than the  $\gamma$ -crystalline forms. Uniform dispersion of particles in polymer was shown through SEM. The results showed that incorporation of CaCO<sub>3</sub> particles increased the modulus and tensile strength of neat PA66 however decreased its elongation at yield and break. Nanosized CaCO<sub>3</sub> was superior to micro-sized CaCO<sub>3</sub> in that it caused higher modulus and strength.

**Keywords:** Polyamide-66, CaCO<sub>3</sub> nanoparticles, nano-composites, optical properties, thermal properties, mechanical properties.

### INTRODUCTION

Polymer composites represent an important class of engineering materials. Although, polymers possess less stability and low module in comparison to metals and ceramics, one of the best ways for modification of their mechanical characteristics is the use of fillers [1, 2]. The incorporation of inorganic fillers into thermoplastics has been widely practiced in industry to extend them and to improve certain properties. Fillers have been used extensively in the past many years to improve properties of polymeric materials. Besides the increment obtained in stiffness, hardness, abrasion resistance, and reduced cost, addition of filler to the polymer also modifies their flow behaviour and consequently its process-ability [3, 4]. One of the most important mineral fillers occupying an important role as particle reinforcing agent in the thermoplastics industry is Calcium Carbonate (CaCO<sub>3</sub>) [5]. In fact, CaCO<sub>3</sub> in most cases is cheaper than other fillers like talc and therefore takes an overwhelming proportion of the filler market in plastics [6]. The production of composites by various methods has become a usual affair since last few years [7]. Nano-composites are a relatively new class of materials with ultrafine phase dimensions, typically of the order of a few nanometres. The objectives for preparation of enhanced performance nano-materials are to obtain

a homogeneous distribution of the nano-particles within the polymer matrix, and to promote a strong interfacial adhesion between the matrix and the nano-filler. Uniform dispersion of the nanometre particles offers a major specific surface area enhancement, compared to conventional reinforcements of micrometre size. As a result, addition of small amount of filler, compared to conventional composites, can induce dramatic changes in host matrix properties [8]. While micron-sized fillers were historically used to lower the cost of relatively expensive polymer resins [9], it is well-understood that incorporation of surface modified inorganic nano-scale fillers (1–100 nm) within a polymer matrix enhances the properties of the polymer dramatically, and the phenomenon has been described as the “nano-effect” [10]. As a consequence, the nano-composite properties are strongly influenced by the nature of the interface between inorganic and polymer matrices. A strong interfacial interaction between the inorganic nano-particles and the polymer matrix can give rise to some unusual properties in these materials [11]. In recent years, demands have increased in using polyamide (PA) to replace certain metals and thermosets in the automotive vehicle and power train systems, and lawn or garden tools with addition of different fillers like fibres, talc and CaCO<sub>3</sub> [12]. Nylon is one of the first commercialized polymers and polyamide-66 having the distinction of highest production [13]. Polyamide-66 (PA66) is a semi-crystalline material that has a combination of strength, flexibility,

---

To whom all correspondence should be sent:  
E-mail: aghadami80@gmail.com; ghadami@iauyasooj.ac.ir

toughness, and abrasion resistance. It is also known for its dye-ability, low coefficient of friction (self-lubricating), low creep, and resistance to solvents, oils, bases, fungi, and body fluids. The applications of polyamide-66 range from textile fibers, membranes, tapes, food packaging to electronics, medical and automotive parts [14].

In this study, the micro-particles (procured in the lab) and nano-particles of CaCO<sub>3</sub> (synthesized using microemulsion method) were used as filler to prepare polyamide-66/CaCO<sub>3</sub> micro- and nano-composites through polymer solution method. The characteristics and properties of the two composites (micro- and nano-) have been compared. The structural and morphological properties of composites were characterized by XRD and SEM. The optical properties of the sample was investigated by FTIR and UV-VIS spectrophotometer. Thermal properties of composites were studied using DSC. The viscosity average molecular weights of polyamide-66 and its micro- and nano-composites were determined using an Ubbelohde viscometer. Universal Testing Machine (UTM) was used to measure mechanical properties (tensile tests) of composites at room temperature according to ASTM-D882.

## EXPERIMENTAL

### *Materials*

CaCO<sub>3</sub> nano-particles with an average size of 33 nm were synthesized via microemulsion route [15]. Micro-CaCO<sub>3</sub> (Merck Company, Germany) particles, procured in the lab with an average size of 2 μm, Dimethyl Sulfoxide (DMSO), 99%, and formic acid (90%) were supplied by Merck Company, Germany. Injection moulding grade polyamide-66 from SRF Limited, India was used to produce micro- and nano-composites.

### *Synthesis of micro- and nano-composites*

Polymer solution method was used for the synthesis of micro- and nano-composites. Effect of the quantity of micro- and nano-particles of CaCO<sub>3</sub> on the synthesized composites was studied for 0, 1, 2 and 3 wt.%. In the following paragraph, the preparation method of polyamide-66/CaCO<sub>3</sub> composites is explained.

Polyamide-66 (PA66), micro- and nano-calcium carbonate particles were first heated in a vacuum oven for 12 hrs at 100°C until any possible residual moisture was removed. Then, polyamide-66 was dissolved in DMSO until a homogeneous solution was obtained. Different amounts of CaCO<sub>3</sub> particles were carefully added to this PA66 solution

under vigorous stirring with a magnetic stirrer bar at room temperature (27°C). The stirring was carried out for 24 hrs under ambient condition of 27°C to get the feed proportion of 1, 2, and 3 wt.% of nano-sized CaCO<sub>3</sub> based on the amount of PA66. Subsequently, the resulting solution was poured onto clean glass plates with side tapes around the glass plates (acting as thin trays) and dried until tack-free in a low-humidity chamber at room temperature. Then, the resultant films were vacuum dried for 24 hrs at 60°C until all the solvent was removed by evaporation delivering polymer nano-composite. All films were prepared for the same time and ambient conditions. Pure PA66 films were prepared in the same manner which also showed opaqueness and milk-white color upon drying of solvent. Conventional composite films were also prepared in the same procedure containing 1, 2, and 3 wt.% of micro-sized CaCO<sub>3</sub>.

### *Filler dispersion analysis*

The synthesized nano-calcium carbonate powders [15] were dispersed in isopropyl alcohol (IPA) and placed in an ultrasonic bath to ensure fine dispersion. Two to three drops were then placed on a filter paper and the CaCO<sub>3</sub> nano-particles were observed under a Transmission Electron Microscope, TEM, (JEOL JEM-2100F, Japan) at 120 KV. The average primary particle size of the nano-particles was then determined from the TEM photomicrograph. The phase morphology of the nylon-66/calcium carbonate nano-composites was examined using a Scanning Electron Microscope (SEM) that is expressed in the next section.

### *Characterization of the synthesized composites*

*X-ray diffraction (XRD) Analysis:* the influence of micro- and nano-CaCO<sub>3</sub> particles on the crystal structure of polyamide-66 was studied using a Rigaku X-ray Powder Diffractometer with Cu anode (Cu K $\alpha$  radiation,  $\lambda=1.54186 \text{ \AA}$ ) in the range of  $5^\circ \leq 2\theta \leq 30^\circ$  and at 30 kV and at a scanning rate of 4°/min.

*Scanning Electron Microscopy (SEM) Analysis:* Scanning Electron Microscope (SEM-EDS, Carl Zeiss: EVO40) at 20 kV was used to characterize the dispersion and agglomeration of micro- and nano-CaCO<sub>3</sub> particles inside the polyamide-66 matrix. The samples were sputter-coated (Sputter Coater: POLARON-SC7640) with a thin layer (10–20 nm) of gold palladium. The coating was carried out by placing the specimen in a high vacuum evaporator and vaporizing the metal held in a heated tungsten basket. In addition, energy-

dispersive X-ray spectroscopy (EDS) was also used to reveal the relative quantities of the different elements present in the compounds.

**Fourier Transform Infrared Spectroscopy (FTIR) Analysis:** FTIR spectroscopy is used for the identification of polymers and additives, study of coupling effects, conformational studies, crystallinity and end group analysis. FT-IR spectra were recorded with an Interspec-2020 (SPECTROLAB, UK) Spectrophotometer using KBr pellets in order to make small tablets; the analyses were conducted between 400 a 4000 cm<sup>-1</sup>.

**Optical Absorption Analysis:** a direct and simple method for probing the band structure of composite materials is to measure the absorption spectrum. The optical absorbance A(v) spectra for the composites were measured using a Ultraviolet-Visible (UV-VIS) Double Beam Spectrophotometer (Perkin Elmer Precisely: Lambda-35) at room temperature in the wavelength range 200-800 nm. The absorption coefficient α(v) was calculated from the absorbance A(v). After correction for reflection, α(v) was calculated using the relation (equation-1):

$$I = I_0 \exp(-\alpha x), \quad (1)$$

Hence,

$$\alpha(v) = \frac{2.303}{x} \log\left(\frac{I_0}{I}\right) = \frac{2.303}{x} A(v), \quad (2)$$

Where, I<sub>0</sub> and I are the incident and transmitted intensity, and x is the thickness of the cuvette. The relationship between fundamental absorption and optical energy gap is given by equation-3:

$$E_{opt} = \frac{hc}{\lambda}, \quad (3)$$

Here, c is the velocity of light. At high absorption coefficient levels for non-crystalline materials, it can be related to the energy of the incident photon by the following relation, equation-4:

$$\alpha(v) = \beta(hv - E_{opt})^n, \quad (4)$$

Where, β is a constant and the exponent, n can assume values of 0.5, 1, 2, 3, and 3/2. For allowed indirect transition, the exponent takes the values 1, 2, and 3 [16]. At low absorption levels (in the range of 1–10<sup>-4</sup> cm<sup>-1</sup>), the absorption coefficient α(v) is described by the Urbach formula [17], equation-5:

$$\alpha(v) = \alpha_0 \exp\left(\frac{hv}{E_U}\right), \quad (5)$$

Where α<sub>0</sub> is a constant and E<sub>U</sub> is an energy term which is interpreted as the width of the tail of localized state of the mobility gap (forbidden band).

**Differential Scanning Calorimetry (DSC):** The degree of crystallinity of polyamide-66 and its micro- and nano-composites were determined using

a Thermal Analysis Apparatus (DSC-60 Shimadzu, Japan). The heating scans were recorded in the temperature range 20-300°C at a heating rate of 10°C/min under nitrogen atmosphere. The degree of crystallinity (X<sub>c</sub>) of polyamide-66 and its composites was calculated from the heat of fusion (ΔH<sub>m</sub>) of the specimen using equation-6:

$$X_c = \frac{\Delta H_m}{\Delta H_m^0 (1 - W_f)} \times 100 \quad (6)$$

Where W<sub>f</sub> is the weight fraction of filler and ΔH<sub>m</sub><sup>0</sup> is the heat of fusion for virgin (100% pure) crystalline PA66 and its value is reported to be 196 J.g<sup>-1</sup> [13].

**Determination of Molecular Weight:** The viscosity average molecular weights of sample were determined using an Ubbelohde viscometer. Relative viscosity (defined as the ratio of the viscosity of a polymer solution to that of the solvent) was calculated by the ratio of torque values. Intrinsic viscosity was calculated from relative viscosities, equations 7, 8 & 9 [18].

$$\eta_{specific} = \eta_{relative}^{-1}, \quad (7)$$

$$\eta_{reduced} = \frac{\eta_{specific}}{C}, \quad (8)$$

$$\eta_{intinsic} = \lim(\eta_{reduced})^c \rightarrow 0, \quad (9)$$

The intrinsic viscosity [η], dl/g, was measured in formic acid at 25°C and the viscometric average molecular weight (M<sub>v</sub>), g/mol, was calculated from the intrinsic viscosity using the Mark–Houwink relation, a relation between viscosity and molecular weight given by equation 10.

$$[\eta] = KM_v^\alpha, \quad (10)$$

Where K and α are constants relating to structure of the solvent, and M<sub>v</sub> is the viscosity average molecular weight. The constants K and α used for the polyamide-66/formic acid system at 25°C are 35.3 × 10<sup>-5</sup> dl/g and 0.786, respectively [19].

**Mechanical Properties (Tensile Tests):** Tensile strength, Young's modulus and percent elongation at yield and break were measured at room temperature according to ASTM-D882 [20] on Zwick 1445 Universal Testing Machine (UTM). The test specimen (film) dimension was 7×0.8×0.09 cm<sup>3</sup> (Length × Width × Thickness). For each composite type, seven specimens were used and the average value of three replicated tests was taken for each composition. Subsequently, the mean values and their standard deviations were calculated. The test specimen gauge length was 5.1

cm and crosshead speed for the film testing was 0.10 cm/min.

## RESULTS AND DISCUSSION

### The used micro- and nano-particles in the Nylon-66 matrix

Fig. 1 shows the TEM photomicrograph of the nano-filler used in this study. The average primary particle size the stearic acid coated nano-CaCO<sub>3</sub> filler was measured to be about 33 nm. This image reveals that most of the coated CaCO<sub>3</sub> nano-particles are quasi-spherical and have rough surface. The nano-particles have a strong tendency to form agglomerates due to their high surface energy which is a result of the small particle size [15].

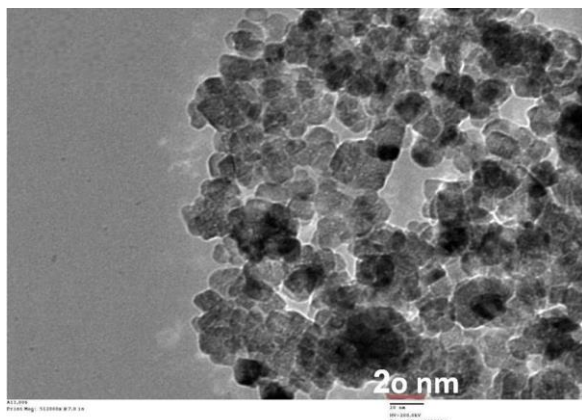


**Fig. 1.** TEM photomicrograph of the nano-CaCO<sub>3</sub> particles used in this study [15].

### XRD analysis

Polyamide-66 (PA66) is a polycrystalline polymer in which triclinic  $\alpha$ -crystalline and pseudo-hexagonal  $\gamma$ -crystalline are the most important phases. The triclinic  $\alpha$ -phase structure at room temperature transforms into  $\gamma$ -phase structure at elevated temperatures [21]. Liu, et al. (2007) have reported that even though, the stable crystalline form of PA66 at room temperature is in the  $\alpha$ -crystalline,  $\gamma$ -crystalline forms can also co-exist along with the  $\alpha$ -crystalline form depending on processing conditions [22]. XRD measurements were used to investigate the influence of CaCO<sub>3</sub> particles on the crystal structure of polyamide-66. The XRD patterns of PA66 and PA66/CaCO<sub>3</sub> micro- and nano-composites are shown in Fig. 2.

It is well documented that the crystalline structure of a semi-crystalline thermoplastic has significant effect on the thermal and mechanical properties. Furthermore, XRD results of composites have suggested that CaCO<sub>3</sub> particles are found in the amorphous phase of the semi-crystalline thermoplastic. It has been found that the  $\alpha$ -

crystalline form is thermodynamically more stable than the  $\gamma$ -crystalline forms at room temperature [22, 23]. As shown in **Fig. 2**, the XRD pattern of neat PA66 (PA66 with 0 wt.% CaCO<sub>3</sub>) displays two strong diffraction peaks at  $2\theta=19.232$  and  $23.280^\circ$  corresponding to the (100) and (010) (110) doublet of the  $\alpha$ -crystalline structure. Furthermore, a small peak at  $12.634^\circ$  is associated with the (002) plane of the  $\gamma$ -crystalline structure. It can be seen from **Fig. 2** that with increasing the content of CaCO<sub>3</sub> particles within polyamide-66 matrix, the  $\gamma$  crystalline form tends to disappear. Thus, it may be said that calcium carbonate particles form a PA66 crystal thermodynamically more stable with the reduction of the metastable  $\gamma$  crystalline phase within the polymeric matrix and forming only an  $\alpha$  crystalline structure. The d-spacing between the planes in the atomic lattice was calculated using Bragg's law [24, 25]:

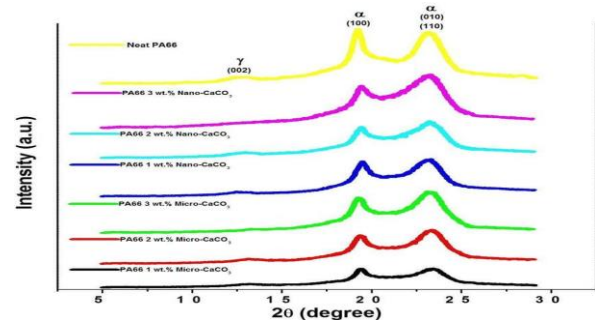


**Fig. 2.** XRD patterns of neat PA66 and PA66/micro- and nano-CaCO<sub>3</sub> composites: 1, 2 and 3 wt. % CaCO<sub>3</sub> micro- and nano-particles.

It has been obtained that the presence of CaCO<sub>3</sub> particles does not influence the d-spacing of the  $\alpha$ - and  $\gamma$ -crystalline forms of polyamide-66. The d-spacings of  $\alpha$  (100),  $\alpha$  (010) (110) and  $\gamma$  (002) for all nano-composites are 0.46, 0.38 and 0.69 nm, respectively. This may be interpreted as follows: each set of miller planes with a unique d-spacing can give rise to a distinct diffraction peak in the x-ray diffraction pattern. When two or more sets of miller planes have the same d-spacing, the diffraction peaks fall at the same position (angle) in the diffraction pattern. This point is supported by Yasmin and Daniel, 2004 [26]. Thus, the non-variation of the d-spacings of the  $\alpha$ -crystalline forms demonstrates that CaCO<sub>3</sub> particles may be found in the free volume of PA66. The incorporation of surface modified CaCO<sub>3</sub> filler in the polymer chains causes the increase of the amorphous region and the particles can have larger surface area in contact with the polymer, especially the nano-particles that have very small size scale and immense surface area per unit volume. This

means that there are more sites available for filler–filler and matrix–filler interactions and adhesions.

#### *Scanning electron microscopy (SEM) analysis*

The dispersion of the particles inside the bulk PA66 was investigated using SEM. It is known that the dispersion of filler in the polymer matrix can have significant effect on the mechanical properties of the composites. However, the dispersion of inorganic filler in a thermoplastic is not an easy process. The process becomes more intricate when nano-particles are used as filler, because they have strong tendency to agglomerate. It is reported that a good dispersion can be achieved by surface modification of the filler particles [27]. It is pertinent to state that in this study, it was tried to take those images of samples through SEM that show the cavities on the surface of the polymer. The aggregation of polyamide-66 particles seen in these images is attributed to the size of applied magnifications. Referring to the figure cited in the inset, Fig. 3(b), the normal situation of the presence of the micro-particles in the polymer chains may be observed through different resolution (resolution of 5 $\mu$ m). Fig. 3(a) shows the SEM micrograph of neat PA66. The uniform dispersion of 1, 2, and 3 wt. % surface modified micro- and nano-CaCO<sub>3</sub> within PA66 are evidenced from SEM images as shown in Figs. 3(b)-(g). The Energy dispersive spectrometer (EDS) analysis, Fig. 3(h), shows the presence of CaCO<sub>3</sub> particles in the polymer composites. The weight percentage of constituents of polymer composites may also be found. Figs. 3(d) and (g) indicate the SEM micrograph of well-distributed 3 wt.% of surface modified micro- and nano-CaCO<sub>3</sub> particles within PA66, respectively. A similar degree of the CaCO<sub>3</sub> distribution is also observed for lower weight fraction of CaCO<sub>3</sub> (e.g., 1 and 2 wt. %).

It is clearly noticed from these figures that both types of surface modified, micro- and nano-particles are covered to the PA66 matrix. Moreover, nano-fillers appear homogeneously dispersed into polymer. Referring to Fig. 3(a), cavities can be found on the surface of the neat PA66. Some of these cavities which are occupied by micro-CaCO<sub>3</sub> particles are shown in Figs. 3(b) - (d).

Cavitations are also found on the surface of PA66/micro-CaCO<sub>3</sub> composites, as cited in Figs. 3(b)-(d). However, since no cavity is observed on the surface of PA66/nano-CaCO<sub>3</sub> composites, as noticed in Figs. 3(e) - (g), the presence of nano-particles must be more responsible than micro-particles for the cavitations. The figures cited in the inset, Figs. 3(e)-(g), also show uniform dispersion

of CaCO<sub>3</sub> nano-particles in PA66 matrix through different resolution (resolution of 5 $\mu$ m). In the nano-composites containing CaCO<sub>3</sub>, Figs. 3(e) - (g), the particles are found better covered to the PA66 matrix and have larger surface area in contact with the polymer matrix compared to micro-CaCO<sub>3</sub> particles. In addition, cavities are present at the interface, suggesting that the coating of CaCO<sub>3</sub> promotes adhesion between the particles and PA66 matrix thus improving the compatibility between the phases.

#### *Fourier transform infrared spectroscopy (FTIR) analysis*

FTIR can be used to detect amorphous or crystalline CaCO<sub>3</sub> on PA66 surfaces. FTIR spectra taken for neat PA66, PA66/CaCO<sub>3</sub> micro- and nano-composites are shown in Figs. 4 to 10. The band assignments for PA66 are well documented in the literature [28]. Fourier-transform IR confirmed the chemical structure of the PA66, Fig. 4, showing absorptions for all required chemical groups: N-H stretch at 3305.52 cm<sup>-1</sup>, C-H stretch at 2865.02-2936.45 cm<sup>-1</sup>, Amide-I at 1638.76 cm<sup>-1</sup>, and Amide-II at 1539.55 cm<sup>-1</sup>. The band at N-H stretching and C=O stretching strongly depend on hydrogen bonding interaction between the PA66 chains, these results are supported by the reported literature [29]. CaCO<sub>3</sub> forms a complex with C-H groups in polyamides and break the hydrogen bonds between PA66 chains, as can be inferred from Figs. 5 to 10. Therefore it is expected to see a shift in the vibrational bands associated with C-H stretching vibration. For instance, the fundamental bands and probable assignments for neat PA66 and PA66/Nano-CaCO<sub>3</sub> composite consisting 3 wt.% CaCO<sub>3</sub> nano-particles are given in Tables 1 and 2 respectively.

Structural changes were observed in the FTIR spectra after the addition of filler in PA66. There were some significant changes observed in the IR absorption of the C-H region at 1478.87 cm<sup>-1</sup> (Strongest peak relating to CaCO<sub>3</sub> nano-particles) between the filled and unfilled PA66. Changes in the peaks proved that the addition of filler in the matrix affects the transmittance of that polymer. It means that the interfacial effect would be a dominant factor where there is direct binding of the polymer and the filler. These results are in good agreement with reported results by Basilia, et al. (2007) [30]. The exposed thick PA66 sample has an absorbance peak at 877 cm<sup>-1</sup>. This peak is due to the absorbance of the CO<sub>3</sub> group and indicates the presence of CaCO<sub>3</sub>; this point is supported by Suel, et al. (2004) [31]. If N-H bonds shift to higher

frequency the red shift will be caused by these bonds but in the reverse case the blue shift is caused by them due to the reduction in bond order. The primary motivation for determining the molecular structure of a polymer using FTIR spectroscopy is to relate the structures to the

performance properties of the polymer in end use. If the polymer chains are completely characterized and the structural basis of its properties are known, the polymerization reaction can be optimized and controlled to produce the optimum properties from the particular chemical system [32].

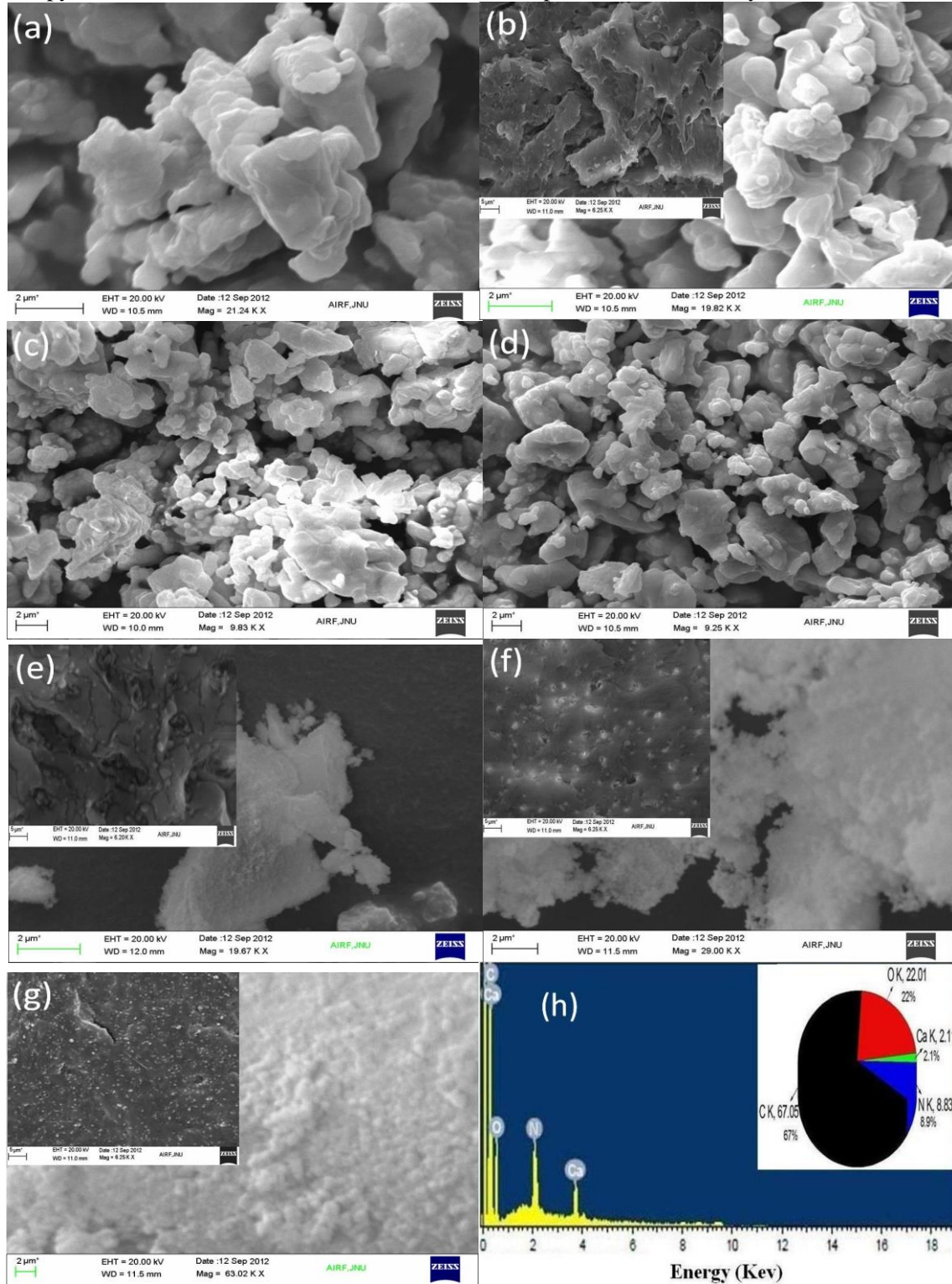


**Fig. 3.** SEM images of (a): neat polyamide-66 (PA66); PA66/micro- $\text{CaCO}_3$  composite (b): 1 wt. % micro- $\text{CaCO}_3$  (c): 2 wt. % micro- $\text{CaCO}_3$  (d): 3 wt. % micro- $\text{CaCO}_3$ ; PA66/nano- $\text{CaCO}_3$  composite (e): 1 wt. % nano- $\text{CaCO}_3$  (f): 2 wt. % nano- $\text{CaCO}_3$  (g): 3 wt. % nano- $\text{CaCO}_3$  (h): Energy-dispersive x-ray (EDS) spectra of PA66/ $\text{CaCO}_3$  composites; (insets show resolution of 5 μm)

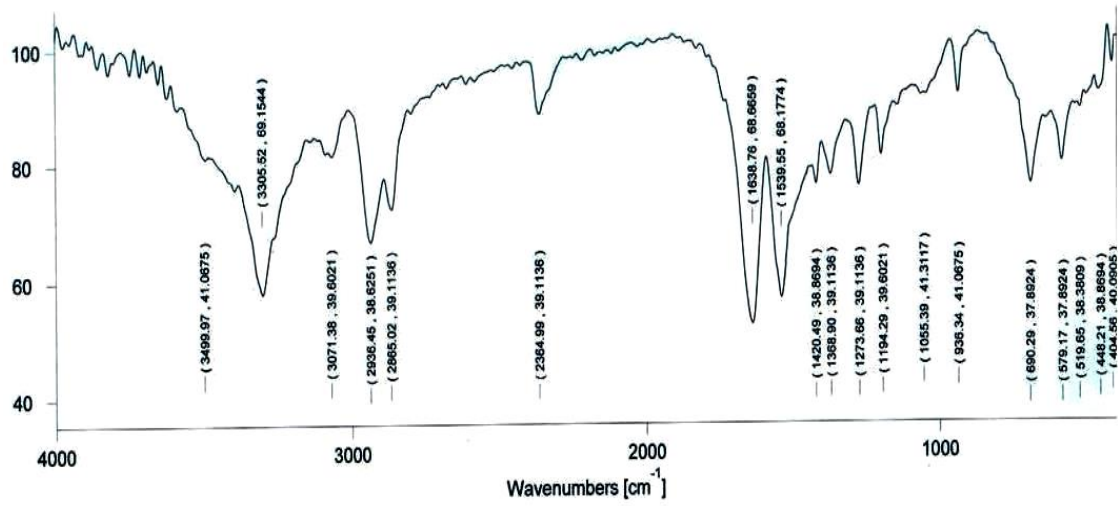


Fig. 4. FT-IR spectrum of neat nylon-66 (PA66).

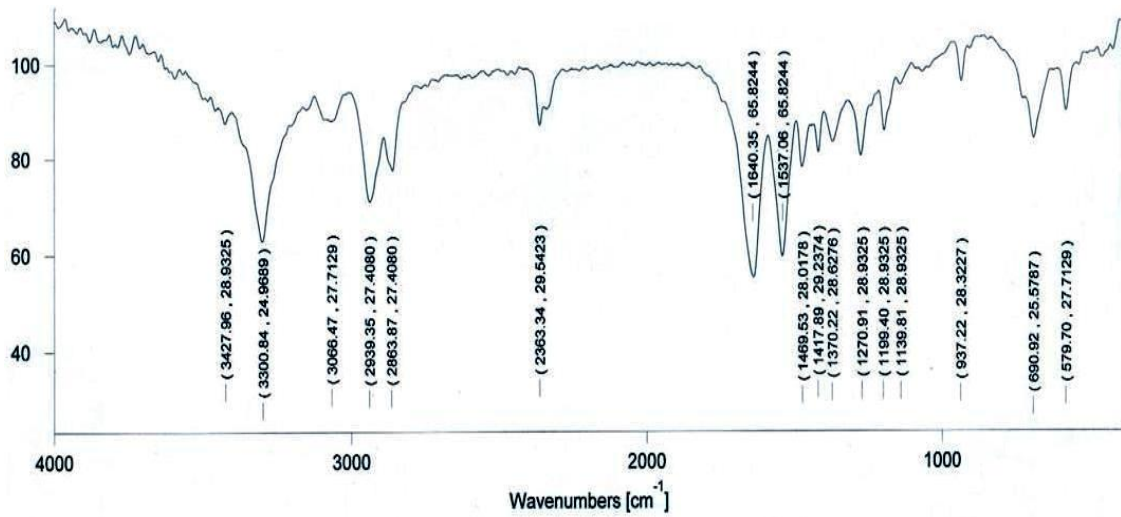


Fig. 5. FT-IR spectrum of PA66/Micro- $\text{CaCO}_3$  composite: 1 wt.% micro- $\text{CaCO}_3$  particles.

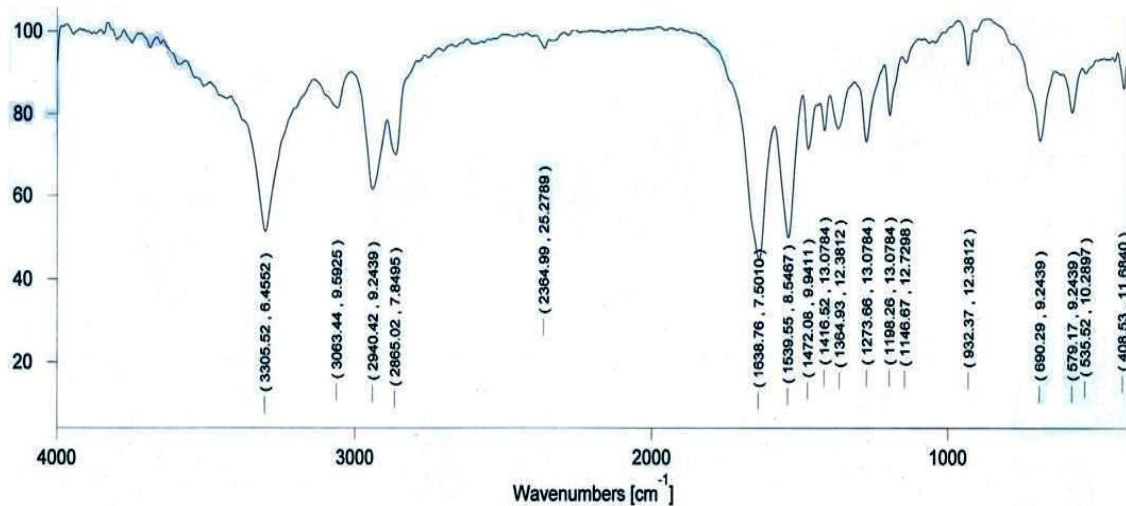


Fig. 6. FT-IR spectrum of PA66/Micro- $\text{CaCO}_3$  composite: 2 wt.% micro-  $\text{CaCO}_3$  particles.

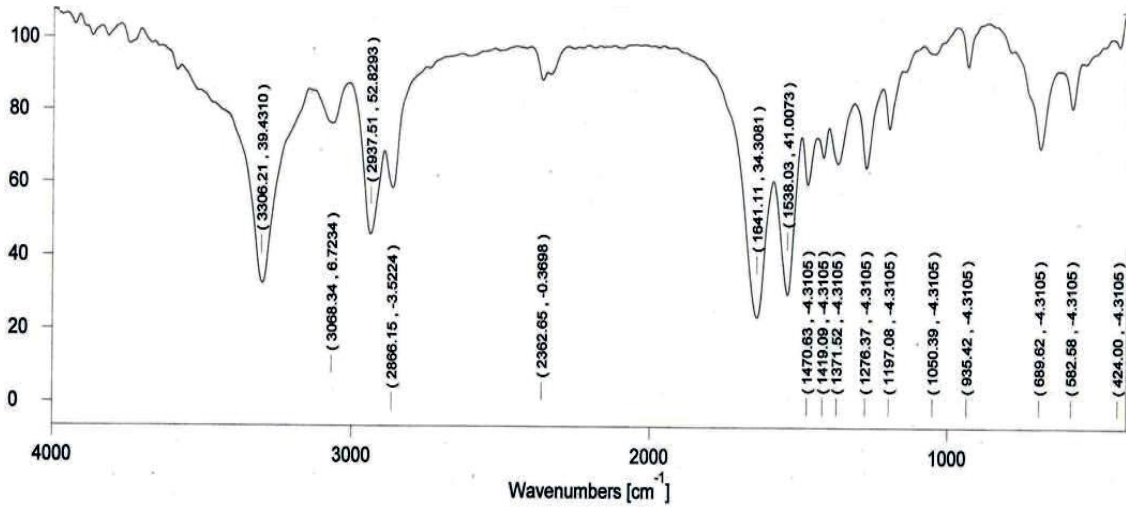


Fig. 7. FT-IR spectrum of PA66/Micro-CaCO<sub>3</sub> composite: 3 wt.% micro-CaCO<sub>3</sub> particles.

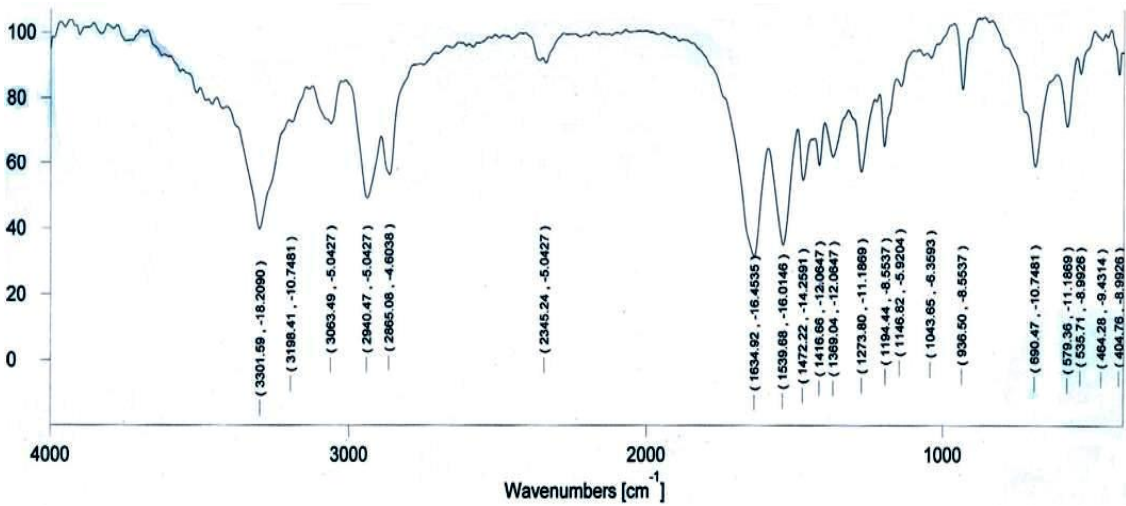


Fig. 8. FT-IR spectrum of PA66/Nano-CaCO<sub>3</sub> composite: 1 wt. % nano-CaCO<sub>3</sub> particles.

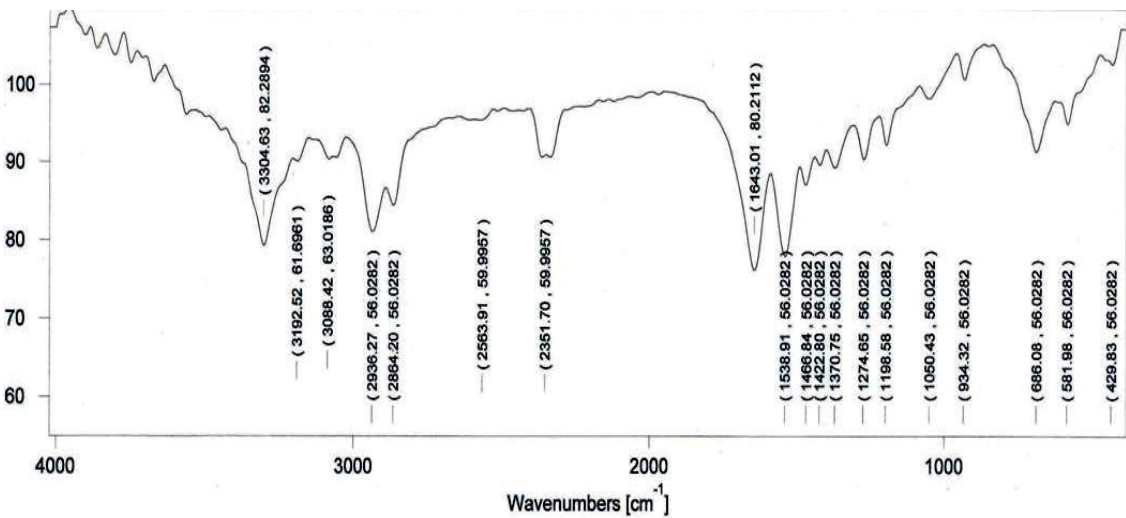


Fig. 9. FT-IR spectrum of PA66/Nano-CaCO<sub>3</sub> composite: 2 wt.% nano-CaCO<sub>3</sub> particles.

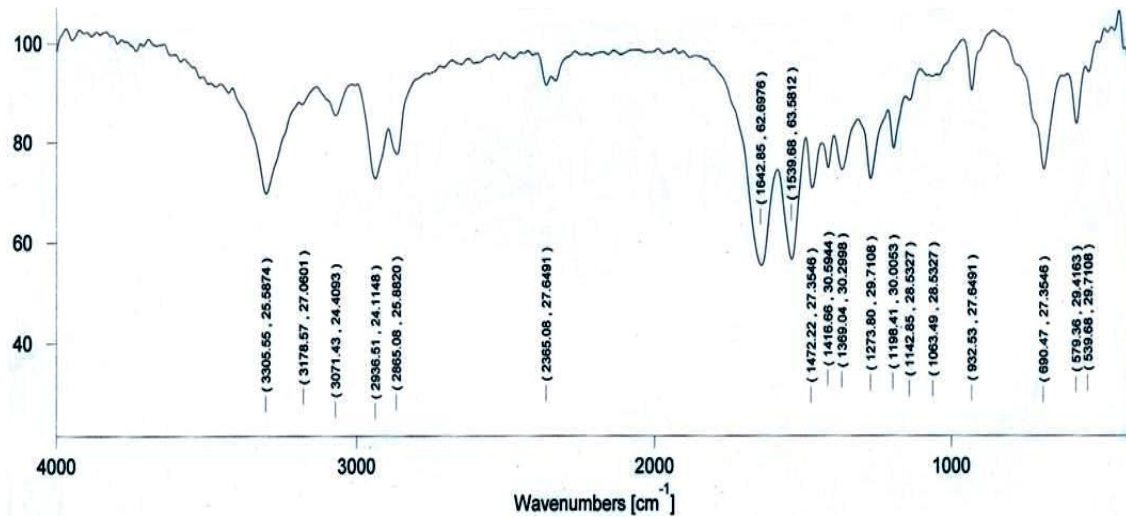


Fig. 10. FT-IR spectrum of PA66/Nano-CaCO<sub>3</sub> composite: 3 wt.% nano-CaCO<sub>3</sub> particles.

Table 1. FT-IR spectra and assignment of PA66.

Wavenumbers (cm <sup>-1</sup> )	Assignment
3305.52	N-H stretching
3080.11	C-H asymmetric stretching
3071.38	C-H symmetric stretching
2936.45	CH <sub>2</sub> asymmetric stretching
2865.02	CH <sub>2</sub> symmetric stretching
1745.03	C=O stretching
1638.76	Amide I band
1539.55	Amide II band/CH <sub>2</sub> asymmetric deformation
1420.49	N-H deformation/CH <sub>2</sub> scissoring
1368.90	Amide III band/CH <sub>2</sub> wagging
1149.29	CCH symmetric bending/CH <sub>2</sub> twisting
1128.20	CCH symmetric bending
936.34	C-C stretching
690.29	N-H wagging/CH <sub>2</sub> rocking
606.23	C-C bending
579.17	O=C-N bending

Table 2. FT-IR spectra and assignment of PA66/CaCO<sub>3</sub> nano-composite: 3 wt. % nano-CaCO<sub>3</sub> particles.

Wavenumbers (cm <sup>-1</sup> )	Assignment
3305.55	N-H stretching
3178.57	C-H asymmetric stretching
3091.43	C-H symmetric stretching
2936.51	CH <sub>2</sub> asymmetric stretching
2865.08	CH <sub>2</sub> symmetric stretching
1745.23	C=O stretching
1642.85	Amide I band
1539.68	Amide II band/CH <sub>2</sub> asymmetric deformation
1472.22	N-H deformation/CH <sub>2</sub> scissoring
1369.04	Amide III band/CH <sub>2</sub> wagging
1142.85	CCH symmetric bending/CH <sub>2</sub> twisting
1128.10	CCH symmetric bending
932.53	C-C stretching
690.47	N-H wagging/CH <sub>2</sub> rocking
606.23	C-C bending
579.36	O=C-N bending

*Optical absorption analysis*

Optical absorption occurs by transition of electrons and holes between electronic states (bands, tail and gap states) and the energy-band gap is the energy needed to break a bond in the crystal. When a band is broken, the electron has enough energy to leave the valence band and jump to conduction band. The width of the band gap determines the type of material (conductor, semiconductor and insulator). Optical absorption studies on neat PA66 and PA66/CaCO<sub>3</sub> micro- and nano-composites recorded at room temperature and presented in Fig. 11 were carried out to obtain energy-band gaps of the samples.

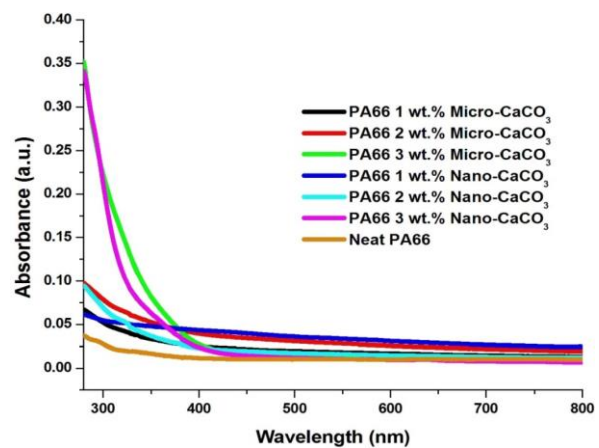
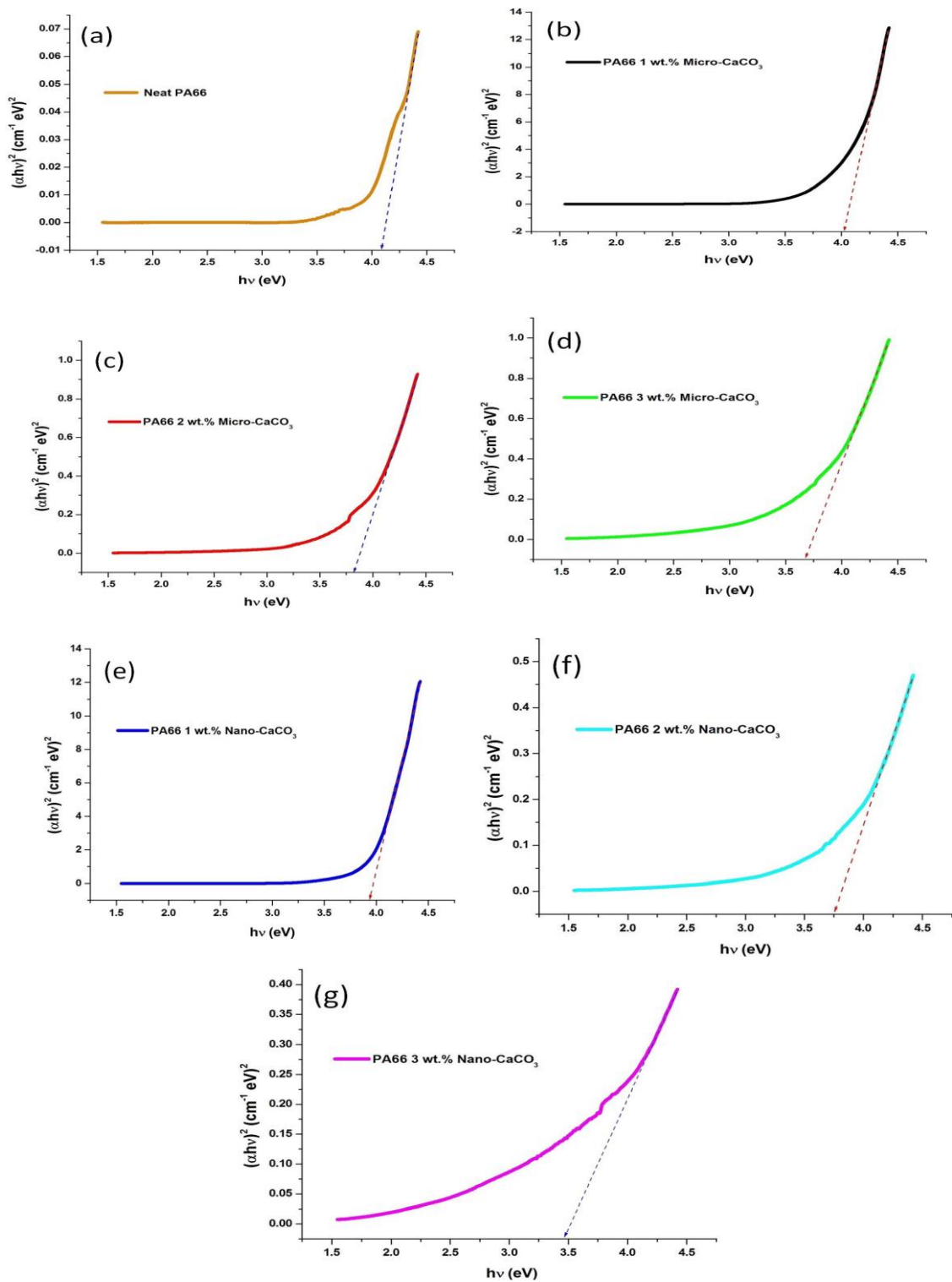
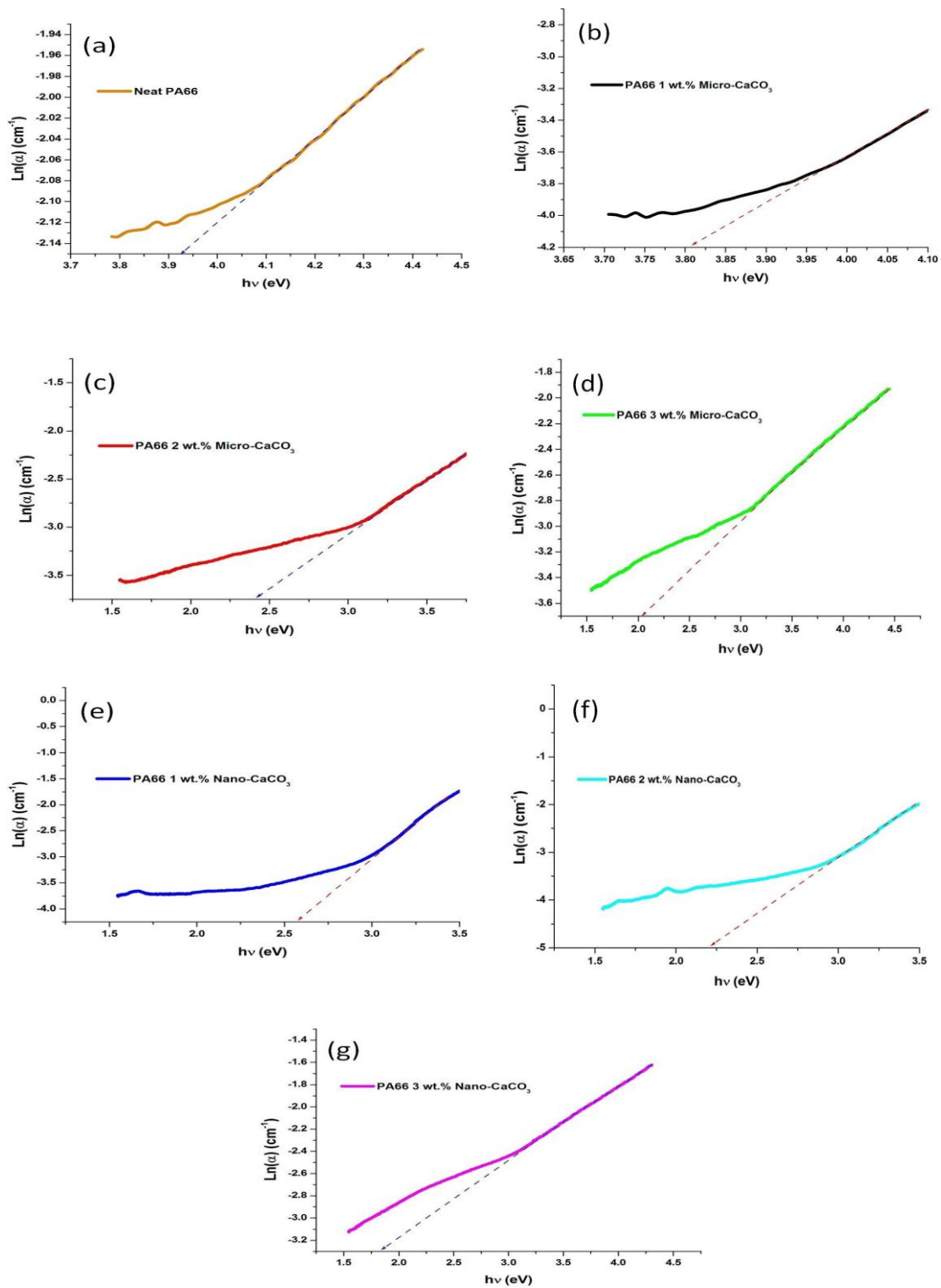


Fig. 11. The optical absorption spectra for neat PA66 and PA66/CaCO<sub>3</sub> micro- and nano-composites.



**Fig. 12.** Evaluations of  $E_{\text{opt}}$  from optical absorption spectra of (a): neat polyamide-66 (PA66); PA66/micro- $\text{CaCO}_3$  composite (b): 1 wt. % micro- $\text{CaCO}_3$  (c): 2 wt. % micro- $\text{CaCO}_3$  (d): 3 wt. % micro- $\text{CaCO}_3$ ; PA66/nano- $\text{CaCO}_3$  composite (e): 1 wt. % nano- $\text{CaCO}_3$  (f): 2 wt. % nano- $\text{CaCO}_3$  (g): 3 wt. % nano- $\text{CaCO}_3$ .



**Fig. 13.** The linear dependence of  $\ln\alpha$  on  $h\nu$  and estimation of Urbach's energy for (a): neat polyamide-66 (PA66); PA66/micro- $\text{CaCO}_3$  composite (b): 1 wt. % micro- $\text{CaCO}_3$  (c): 2 wt. % micro- $\text{CaCO}_3$  (d): 3 wt. % micro- $\text{CaCO}_3$ ; PA66/nano- $\text{CaCO}_3$  composite (e): 1 wt. % nano- $\text{CaCO}_3$  (f): 2 wt. % nano- $\text{CaCO}_3$  (g): 3 wt. % nano- $\text{CaCO}_3$ .

**Table 3.** The estimated optical data of neat PA66 and PA66/CaCO<sub>3</sub> composites.

Material	Wavelength (nm)	Absorbance (arb units)	$E_{opt}$ (eV)	$E_U$ (eV)
Neat PA66	280	0.029	4.10	0.25
PA66/1 wt. % micro CaCO <sub>3</sub>	280	0.067	4.03	0.26
PA66/2 wt. % micro CaCO <sub>3</sub>	280	0.098	3.82	0.41
PA66/3 wt. % micro CaCO <sub>3</sub>	280	0.354	3.68	0.49
PA66/1 wt. % nano CaCO <sub>3</sub>	280	0.061	3.93	0.39
PA66/2 wt. % nano CaCO <sub>3</sub>	280	0.095	3.76	0.45
PA66/3 wt. % nano CaCO <sub>3</sub>	280	0.343	3.47	0.55

**Table 4.** Summary of DSC heat scan results of neat PA66 and PA66/CaCO<sub>3</sub> micro- and nano-composites.

Sample	Wt. % of loading	$T_m$ (°C)	$\Delta H_m$ (J/g)	Crystallinity (%)
Neat PA66	0	262.14	85.14	44.78
PA66/Micro-CaCO <sub>3</sub> composite	1	260.90	84.05	44.21
	2	254.80	81.46	42.41
	3	246.90	73.13	41.38
PA66/Nano-CaCO <sub>3</sub> composite	1	259.40	82.59	42.99
	2	247.30	75.47	41.75
	3	242.70	70.77	39.54

It may be deduced from the curves in this figure that the addition of CaCO<sub>3</sub> particles in polyamide-66 increases the absorbance of the composites. In order to evaluate the energy band gaps for the composites, plots of  $(\alpha h\nu)^2$  versus photon energy  $(h\nu)$  were obtained and are shown in Figs. 12-(a) - (g). The best fit to the absorption spectra were obtained when the value of  $n$  used was equal to 0.5, suggesting that the electron transition allowed direct transition for these nano-composite samples. It can be seen that the plots are linear in the region of strong absorption near the fundamental absorption edge. Thus, the absorption takes place through direct transition. The band gap obtained by extrapolating the linear part to zero of the ordinate are also indicated in the figures. This lead to the evaluation of the band gaps,  $E_{opt}$ , while slope gives the value of constant  $\beta$ . The factor  $\beta$  depends on the transition probability and can be assumed to be constant within the optical frequency range [33]. Adding CaCO<sub>3</sub> in PA66 matrix may cause the localised states of different colour centres to overlap and extend in the mobility gap. This overlap may give an evidence for decreasing energy gap when adding CaCO<sub>3</sub> in the polymer matrix.

The Urbach formula was used to calculate the width of the Urbach's tail of the localised states due to the defect levels in the transition gap, as suggested by Davis and Mott, 1970 [16]. The Urbach's tail is generally attributed to the disorder in the material that leads to another tail in the valence and conduction bands [34]. It was reported that Urbach's tail is often observed in crystalline and amorphous materials [35]; therefore the Urbach energy ( $E_U$ ) can be used as a parameter to

determine the optimum growth conditions of these materials. The origin of  $E_U$  is considered as thermal vibrations in the lattice, as reported by Zaki, 2008 [33]. The logarithm of the absorption coefficient ( $\ln\alpha$ ) was plotted as a function of the photon energy  $(h\nu)$  for composites as presented in Figs. 13-(a) to (g). The reciprocal of the slopes of the curves yields the magnitude of width of the band tail,  $E_U$ . The values of energy band gaps,  $E_{opt}$  and Urbach's energy,  $E_U$  for the pure PA66 and PA66/CaCO<sub>3</sub> composites obtained from the cited figures above are summarised in Table 3. A glance at the data presented in the table reveals that addition of CaCO<sub>3</sub> particles in PA66, results in the decrease of energy-band gaps of the composites; the values being less than that for neat PA66. Highest reduction of energy-band gap was related to PA66/nano-CaCO<sub>3</sub> with 3 wt. % CaCO<sub>3</sub> nanoparticles. It was also observed that the Urbach's tail for pure PA66 is less than that for PA66/CaCO<sub>3</sub> composites. The decrease in the Urbach's energy in case of PA66 may be due to the decrease in the crystalline nature of the polymer.

#### Differential Scanning Calorimetry (DSC)

The influence of the micro- and nano-CaCO<sub>3</sub> in the composites on the crystallization mechanism of the PA66 matrix was studied through differential scanning calorimetry. DSC studies for neat PA66 and PA66/CaCO<sub>3</sub> micro- and nano-composites upon heating provided the glass transition temperature ( $T_g$ ), melting temperature ( $T_m$ ) and degree of crystallinity ( $X_c$ ) and the endotherms are presented in Fig. 14.

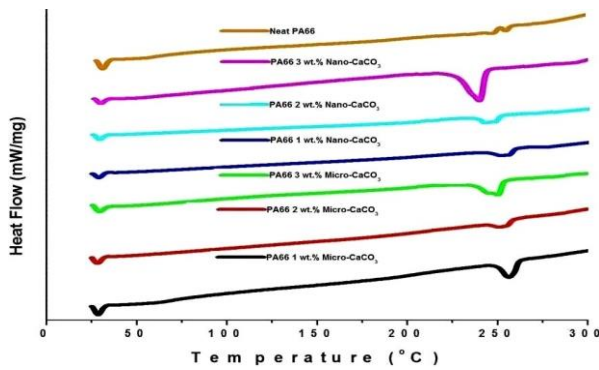


**Fig. 14.** Composite figure showing DSC melting endotherms during the heating scans of neat PA66 and PA66/micro- and nano-CaCO<sub>3</sub> composites.

The DSC scans of the neat PA66 and PA66/CaCO<sub>3</sub> complexes showed a single relaxation temperature ( $T_g$ ) at  $\square\square 30^\circ\text{C}$ . The heat of fusion and melting temperatures obtained from the endotherms are summarised in Table 4. There is an interesting observation in DSC melting endotherm, Fig. 14. Neat PA66 gives two endothermic peaks during the heating ramp, one around 258°C and the other one at 262°C, the first melting peak corresponds to the  $\alpha$ -crystalline phase and a small shoulder peak before the main endothermic peak ( $\alpha$ -crystalline phase) corresponding to  $\gamma$ -crystalline phase of neat PA66, as noticed by other researchers [36, 37]. This observation is also supported by the XRD analysis of the neat PA66 where both  $\alpha$ - and  $\gamma$ -crystalline forms were noticed, Fig. 2 and an explanation given thereof. The percent crystallinity of the PA66 samples was calculated as the ratio of the heat of fusion ( $\Delta H_m$ ) of the sample to the heat of fusion of the pure crystalline at the weight fraction of composite form equation-1. The heat of fusion of pure polyamide is taken as 196 J.g<sup>-1</sup> [13]. It can be observed in Table 4 that the crystallinity of pure PA66 is 44.78% and the addition of CaCO<sub>3</sub> causes decrease in crystallinity and these observations are in accordance with the results obtained from the UV-VIS spectrophotometry.

As a result, heat of fusion decreases when inorganic filler was added. It seems that the modified surface of the CaCO<sub>3</sub> filler increases the amorphous region of polymer chains and is in good agreement with the results reported earlier by Basilia, et al., 2007 [30]. However, the DSC data indicate that incorporation of CaCO<sub>3</sub> results in simultaneous decrease of melting point especially at the higher nano-CaCO<sub>3</sub> content. The incorporation of nano-CaCO<sub>3</sub> into polyamide composites shows lower degree of crystallinity than that of micro-CaCO<sub>3</sub> filled polyamide composite. Analytical results for polymer composites obtained independently DSC studies show that incorporation

of CaCO<sub>3</sub> particles in the polymer matrix improves the thermal stability of the micro- and nano-composites, more so for the latter.

#### Characterization of molecular weight

In a capillary viscometer, the ratio ( $t/t_0$ ) of the flow time,  $t$  of a polymer solution of concentration  $c$  to the  $t_0$  of the pure solvent is proportional to the ratio of their viscosity ( $\eta/\eta_0$ ) if temperature is kept constant and the density does not change with polymer concentration in solution [18]. In this study, molecular weights of the pure and synthesised samples were calculated using intrinsic viscosity values which were determined by the solution viscosity method. The experiments for determining the intrinsic viscosity of polyamide-66 were conducted as follows. Polyamide-66 (1 g) was dissolved in formic acid (50 ml) to form a stock solution (2 g/dl). Other samples of varying concentration were prepared by serial dilution of the stock solution. The samples were poured into the viscometer maintained at 25°C. The time taken for the solution to flow between two points (efflux time) on the viscometer was recorded (efflux time was replicated in triplicate to get an average value). The concentration of the polymer solution and the corresponding efflux time was used to calculate various viscosity values. The reduced viscosity ( $\eta_{\text{reduced}}$ ) values so obtained for each sample were plotted against concentration ( $c$ ), and the best fit through the data provided the intrinsic viscosity. All the concentrations used in this study were in the range of 1.54 – 2.0 g/dl. Finally, the Mark–Houwink formula was used to determine the viscosity-average molecular weight ( $M_v$ ) of samples from the intrinsic viscosity measurements, resulting in a  $M_v \sim 18,000$  g/mol. Therefore, it may be concluded that the presence of CaCO<sub>3</sub> particles is not able to change the structure and molecular weight of PA66.

#### Tensile properties of composites

Tensile properties of the seven pieces of each composite sample were examined using Zwick 1445 Universal Testing Machine (UTM). For each piece of all the micro- and nano-composite samples, the stress-strain ( $\sigma$ - $\epsilon$ ) data was plotted in terms of elongation. For each sample, 2-3 stress-strain ( $\sigma$ - $\epsilon$ ) curves which had significant differences with the others were rejected and the calculation for the tensile properties was done only on the remaining, and the average results were considered as the property of each sample. The calculated values of the Young's modulus of neat PA66 and PA66/CaCO<sub>3</sub> micro- and nano-composites are

plotted in Fig. 15 showing the effect of content of micro- and nano-sized CaCO<sub>3</sub> particles on the modulus of PA66/CaCO<sub>3</sub> composites. It has been widely accepted that doping of the fillers into polymer matrix would improve the mechanical properties of the resulting composites [38, 39]. The addition of the CaCO<sub>3</sub> leads to improvement in stiffness for both the micro-composites and nano-composites. The results shown in Fig. 15 reveal that the Young's modulus of filled polyamide nano-composites is higher than that of micro-CaCO<sub>3</sub>-filled composites. Further, incorporation of CaCO<sub>3</sub> leads to increase in the Young's modulus of polyamide-66 composites in proportion to the increase content of the filler and this observation is attributed to the higher reinforcing effect of nano-particles compared to micro particles. Enhancement of the tensile modulus with increased filler content can be interpreted as follows. In general, adding filler to polymer matrix reduces the mobility of polymer chains which in effect causes more stiffness or higher value of tensile modulus of the polymer composite and also this effect can be raised by increasing the amount of filler.

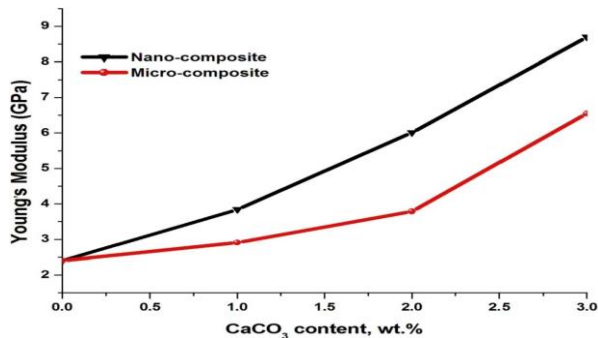


Fig. 15. Effect of filler loading on the Young's modulus of micro- and nano- Polymer composites.

The relationship between weight percentage of filler loading (micro- and nano-CaCO<sub>3</sub>) and strength at yield and break for PA66/CaCO<sub>3</sub> micro- and nano-composites are shown in Figs. 16 and 17. The tensile strength of nano-CaCO<sub>3</sub> filled polyamide composites is recorded higher than that of micro-CaCO<sub>3</sub> filled polyamide composites; the highest loading of the filler (in the range studied) shows the highest tensile strengths of composites and nano-fillers provide higher tensile strength compared to micro-CaCO<sub>3</sub>. This increment in tensile strength is due to uniform dispersion of nano-filler throughout the matrix. The uniform dispersion of nano-CaCO<sub>3</sub> is confirmed from the SEM images shown in Figs. 3(e)-(g). The reason for higher tensile strength of nano-composites is that the nano-sized CaCO<sub>3</sub> particles have larger surface area in contact with the polymer matrix. As

such, the overall bonding strength between the particles and matrix is higher. Thus, it is to be expected that nano-composites could stand higher loading under external forces, as suggested by Zhu, et al., 2006 [40]. When the content of CaCO<sub>3</sub> is low, the micro- and nano-sized CaCO<sub>3</sub> cannot well disperse in the polyamide matrix and agglomerate to form a big cluster and cause a decrease in tensile strength.

Elongation percent of composite samples under stress can be calculated from the relation (equation-11), where  $L_o$  is the initial length of the test specimen, and  $L$  is the final length of sample after applying the stretching force.

$$\text{Elongation Percent} = \frac{L - L_o}{L_o} \times 100, \quad (11)$$

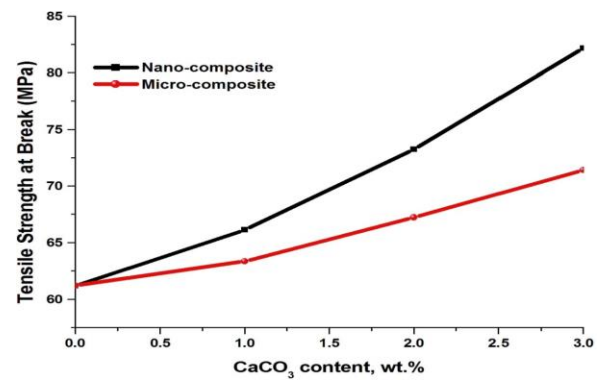


Fig. 16. Variation of tensile strength of micro- and nano-composites with filler loading at break.

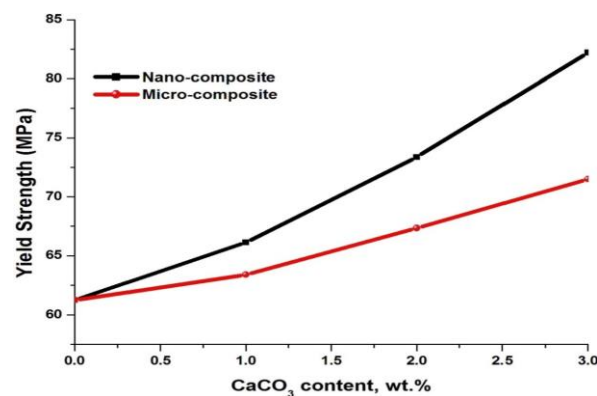
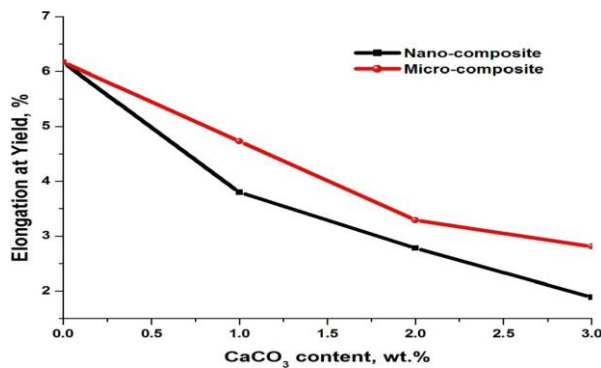


Fig. 17. Variation of tensile strength of micro- and nano-composites with filler loading at yield.

Figs. 18 and 19 show the dependence of elongation at yield and break points, respectively. The incorporation of rigid fillers to polymer matrix reduces the elongation at yield and break. This is a common observation reported by earlier researchers. The results show that with increase in weight percentage of filler loading, elongation at yield and break for micro- and nano-composites

decreases. This might be due to the hard nature of polyamide as well as nano-inorganic filler. Addition of filler decreases the elongation at yield and break of composites. This is due to the increment in numbers of spherulites formation with reduction in size and increase in percentage of filler. This may be attributed to the fact that CaCO<sub>3</sub> particles included into the PA66 matrix restrict the movement of polyamide chains. In other words, with the enhancement in rigidity the ductility of composites decreases; consequently the composites break at lower elongation as explained by Zhu, et al., in 2006 [37].



**Fig. 18.** Variation of elongation of micro- and nano-composites with filler loading at yield.

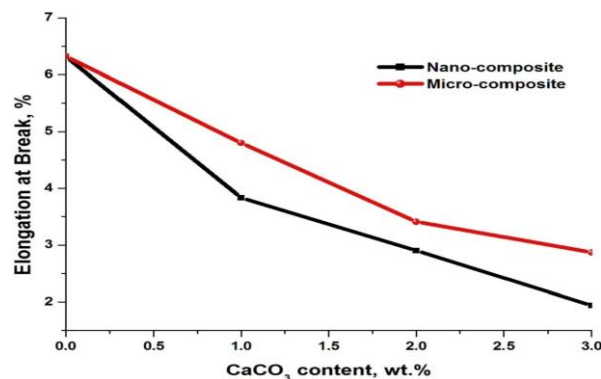


**Fig. 19.** Variation of elongation of micro and nano-composites with filler loading at break.

## CONCLUSIONS

The major findings of this study are summarized as follows:

PA66/CaCO<sub>3</sub> micro- and nano-composites with loading of 0, 1, 2 and 3 wt. % of the micro-particles (~2 μm) and nano-particles (~33 nm) were successfully prepared using polymer solution method. The XRD results of composites have suggested that CaCO<sub>3</sub> particles can form a PA66 crystal thermodynamically more stable with the reduction of the metastable γ-crystalline phase within the polymeric matrix and forming only an α-crystalline structure. SEM results also showed that

both types of surface modified, micro- and nano-particles are covered and quite welded to the PA66 matrix. Moreover, nano-fillers appear homogeneously dispersed into polymer. Fourier-transform infra-red (FT-IR) confirmed the chemical structure of the PA66 showing absorptions for all required chemical groups: N-H stretch at 3305.52 cm<sup>-1</sup>, C-H stretch at 2865.02-2936.45 cm<sup>-1</sup>, Amide-I at 1638.76 cm<sup>-1</sup>, and Amide-II at 1539.55 cm<sup>-1</sup>. There were some significant changes observed in the IR absorption of the C-H region at 1478.87 cm<sup>-1</sup> between the filled and unfilled PA66. Changes in the peaks proved that the addition of filler in the matrix affects the transmittance of that polymer. UV-VIS data proved that addition of CaCO<sub>3</sub> particles in PA66, results in the decrease of energy-band gaps of the composites, and the values are less than that for neat PA66. It was also observed that the Urbach's tail for pure PA66 is less than that for PA66/CaCO<sub>3</sub> composites. DSC data indicated that incorporation of CaCO<sub>3</sub> causes the decrease in crystallinity of composites and also results in simultaneous increase of melting point. Viscometric measurements demonstrated that the presence of CaCO<sub>3</sub> particles is not able to change the structure and molecular weight of PA66. In addition, the results showed that adding CaCO<sub>3</sub> micro- and nano-particles increased the modulus and tensile strength of neat PA66 but decreased its elongation at yield and break. As a result, the nano-CaCO<sub>3</sub> particles cause more effective reinforcement and therefore a stiffer composite.

**Acknowledgements:** This scientific product was extracted through a research project implemented from funding of research projects of Yasouj Branch, Islamic Azad University.

## REFERENCES

1. C.R. Tseng, J.Y. Wu, H.Y. Lee, F.C. Chang, *J. Appl. Polym. Sci.*, **85**, 1370 (2002).
2. J.K. Lim, A. Eggeman, F. Lanni, R.D. Tilton, S.A. Majetich, *Adv. Mater.*, **20**, 1721 (2008).
3. W.C.J. Zuiderduin, C. Westzaan, J. Huetink, R.J. Gaymans, *Polymer*, **44**, 261 (2003).
4. P. Supaphol, P. Thanomkiat, J. Junkasem, R. Dantungee, *Polymer Test.*, **26**, 20 (2007).
5. M.S.F. Samsudin, Z.A. Mohd Ishak, S.S. Jikan, Z.M. Ariff, *Journal of Applied Polymer Science*, **102**, 5421 (2006).
6. H. Zhang, X. Zeng, Y. Gao, F. Shi, P. Zhang, J.F. Chen, *Ind. Eng. Chem. Res.*, **50**, 3089 (2011).
7. J.K. Pandey, K.R. Reddy, A.P. Kumar, R.P. Singh, *Polymer Degradation and Stability*, **88**, 234 (2005).
8. M. Avella, S. Cosco, M.L. Lorenzo, E.D. Pace, E.M. Errico, *J. Thermal Anal. Calorimetry*, **80**, 131 (2005).

9. D. Wu, X. Wang, Y. Song, R. Jin, *Journal of Applied Polymer Science*, **92**, 2714 (2004).
10. A.J. Crosby, J.Y. Lee, *Polymer Rev.*, **47**, 217 (2007).
11. X. Qiang, Z. Chunfang Y. JianZun, C.S. Yuan, *J. Appl. Polym. Sci.*, **91**, 2739 (2004).
12. S.S. Sonawane, S. Mishra, N.G. Shimpi, *Polymer-Plastics Technology and Engineering*, **49**, 38 (2010).
13. J. Brandrup, E.H. Immergut, *Polymer handbook*, 2<sup>nd</sup> Edition, J. Wiley Sons, New York, 1989.
14. X. Jia, M. Herrera-Alonso, T.J. Mc-Carthy, *Polymer*, **47**, 4916 (2006).
15. J.G.A. Ghadami, M. Idrees, *Iranian Journal of Chemistry and Chemical Engineering*, **32**, 27 (2013).
16. E.A. Davis, N. Mott, *Phil. Mag.*, **22**, 903 (1970).
17. F. Urbach, *Phys. Rev.*, **92**, 1324 (1953).
18. R.B. Seymour, C.E. Carraher, *Polymer Chemistry: An Introduction*, 4<sup>th</sup> Edition, New York, 1996.
19. J. Brandrup, E.H. Immergut, *Polymer Hand book*, Wiley, New York, 1975.
20. R. Brendan, in 'Annual Book of ASTM Standards' 1, ASTM International Publisher, Philadelphia, 2002, , p. 160.
21. K. Hedicke, H. Wittich, C. Mehler, F. Gruber, V. Altstadt, *Composites Science and Technology*, **66**, 571 (2006).
22. Y. Liu, L. Cui, F. Guan, Y. Gao, N.E. Hedin, L. Zhu, H. Fong, *Macromolecules*, **40**, 6283 (2007).
23. Z. Xiang, L. Yu-Bao, Z. Yi, L. Guo-Yu, M. Yuan-hua, L. Hong, *Compos Part A Appl Sci Manuf.*, **38**, 843 (2007).
24. H.P. Klugg, L.E. Alexander, *X-ray diffraction procedures*, John Wiley & Sons, New York, 1974.
25. D. Moore, R.J. Reynolds, *X-ray diffraction and identification and analysis of clay minerals of clay minerals*, 2<sup>nd</sup> Ed., Oxford University Press, U. K, 1997.
26. A. Yasmin, I.M. Daniel, *Polymer*, **45**, 8211 (2004).
27. C.M. Chan, J. Wu, J.X. Li, Y.K. Cheung, *Polymer*, **43**, 2981 (2002).
28. H. Arimoto, *J. Polym Sci, Part A*, **2**, 2283 (1964).
29. M. I. Kohan 'Nylon Plastics', John Wiley & Sons, New York, 1973.
30. B.A. Basilia, M.E.G. Panganiban, A.A.V. Collado, M.O.D. Pesigan, P.A. De Yro, *Journal of Solid Mechanics and Materials Engineering*, **1**, 564 (2007).
31. S. D. Suel, S. R. Lee, Y. H. Kim, 'Journal of Polymer Science; Part A: Polymer Chemistry', **42**, 4063 (2004).
32. J. Charles, G. R. Ramkumaar S. Azhagiri, S. Gunasekaran, *E-Journal of Chemistry*, **1**, 23 (2009).
33. M.F. Zaki, *Brazilian Journal of Physics*, **38**, 558 (2008).
34. C.W. Greeff, H.R. Glyde, *Physical Reviewer B.*, **51**, 1778 (1995).
35. L. Bai, C. Xu, P.G. Schunemann, K. Nagashio, R.S. Feigelson, N.C. Giles, *J. Phys.: Condens. Matter*, **17**, 549 (2005).
36. C. Ramesh, A. Keller, S. Eltink, *Polymer*, **35**, 2483 (1994).
37. G.Z. Zhang, T. Watanabe, H. Yoshida, H. Kawai, *Polymer Journal*, **35**, 173 (2003).
38. J. Cayer-Barrioz, D. Ferry, K. Frihi, R. Cavalier G.V. Seguela, *Journal of Applied Polymer Science*, **100**, 989 (2006).
39. H. Hanim, R. Zarina, M.Y.F. Ahmad, Z.A. Mohd, A. Hassan, *Malaysian Polymer Journal*, **3**, 38 (2008).
40. B.K., Zhu, S.H. Xie, Z.K. Xu, Y.Y. Xu, *Compos. Sci. Technol.*, **66**, 548 (2006).